How spotted lanternflies get back on their feet: 3D mechanical modeling explains terrestrial self-righting strategies

Theodore Bien[1§], Benjamin Alexander[1§], Chengpei Li[1§], Natalie Goeler-Slough[1], S. Tonia Hsieh[2], Suzanne Amador Kane [1*]

[1] Physics and Astronomy Department, Haverford College, Haverford, Pennsylvania, United States of America

[2] Department of Biology, Temple University, Philadelphia, United States of America

[§] Contributed equally

[*] Corresponding author

Email: samador@haverford.edu

Running title: How to get back on your feet

Keywords: Locomotion, insects, biomechanics, robophysics, stability

Summary statement

Many animals and robots need to upright quickly when overturned. This study uses 3D models and high-speed video to explain how the invasive spotted lanternfly self-rights effectively on different surfaces.

Abstract

The ability to upright quickly and efficiently when overturned on the ground (terrestrial self-righting) is crucial for living organisms and robots. The emerging field of terradynamics seeks to understand how and why different animals use diverse self-righting strategies. We studied this behavior using high speed multiangle video in nymphs of the invasive spotted lanternfly (SLF, *Lycorma delicatula*), an insect that must frequently recover from falling in its native habitat.

While most insect species previously studied can use wing opening to facilitate overturning, nymphs, like most robots, are wingless. SLFs were highly successful at self-righting (>92% of trials) with no significant difference in the time or number of attempts required for three substrates with varying friction and roughness. These nymphs seldom overturned using the pitching and rolling strategies observed for other insect species, instead primarily flipping upright by rotating around a diagonal body axis. To understand these motions, we used video, photogrammetry and Blender rendering software to create novel, highly realistic 3D models of SLF body poses during each strategy. These models were analyzed using the energy landscape theory of self-righting, which posits that animals use methods that minimize energy barriers to overturning, and inertial morphing, which proposes the animal adjusts its body pose to minimize the rotational inertia during overturning, a theory which has not been applied to self-righting. A combination of both theories was found to explain the observed preferred strategies of this species, indicating the value of using 3D renderings with mechanical modeling for terradynamics and biomimetic applications.

Introduction

Overturned insects benefit from being able to reassume an upright posture quickly and with low metabolic energy investment, thereby mitigating the risk of predation, hunger, and desiccation. This behavior, which is called terrestrial self-righting when the organism reorients to upright while on the ground, has been studied in a wide variety of insects (Li et al., 2019), spiders (O'Donnell, 2018), frogs (Malashichev, 2006), turtles (Domokos and Várkonyi, 2007) and rats (Pellis et al., 1991). Some insects self-right by jumping (Bolmin et al., 2017) or by exerting righting torques on the ground using novel appendages (Brackenbury, 1990; Silvey, 1973), but most do so by using a combination of body, leg and wing motions to rotate about a body axis from supine to upright (Li et al., 2019). These mechanisms have provided important biomimetic inspiration for designing robots that can recover easily from upsets, a particular concern for operating in complex terrains (Saranli et al., 2004).

Ongoing research aims at understanding how the many methods for self-righting used by diverse organisms depend on morphology, locomotor abilities and substrates; for example, Frantsevich documented 20 different modes of self-righting in a study of 116 species of coleoptera (beetles) alone (Frantsevich, 2004). One theoretical model for terrestrial self-righting considers how gravitational potential energy (PE) depends on body pose during a sequence of

motions; this “energy landscape” approach has been used to analyze how animals meet the mechanical requirements for righting (Othayoth and Li, 2021). For example, some turtles have monostatic bodies: their energy landscape has a single minimum in PE corresponding to an upright posture, enabling them to self-right passively using only gravitational forces (Domokos and Várkonyi, 2007). However, most animals either are more stable when overturned or have multiple stable body orientations, requiring active self-righting (i.e., exerting overturning torques on the ground to surmount a PE barrier). Some animals (e.g., frogs, turtles, and spiders) do this quasi-statically by slowly performing work on the substrate (Domokos and Várkonyi, 2007; Malashichev, 2006; O’Donnell, 2018). Others use dynamic strategies, exerting forces rapidly enough to accumulate sufficient kinetic energy (KE) to overcome the PE barrier, either by coordinated motions of the body, leg, wings and tail (Robins et al., 1998; Xuan and Li, 2020a) or by randomly flailing its appendages (Xuan and Li, 2020b). Another alternative is inertial shaping, in which animals adjust their body’s distribution of mass to facilitate flipping over; for example, cockroaches do this by arching their flexible bodies, thereby raising their center of mass (COM)so as to destabilize the overturned pose (Full et al., 1995; Li et al., 2019). These self-righting strategies are not mutually exclusive: e.g., horseshoe crabs rotate their tails rapidly while arching their bodies so as to destabilize their orientation while exerting overturning torques (Silvey, 1973).

Biological systems have inspired novel methods for robot self-righting based on coordinated leg motions (Saranli et al., 2004), wings (Li et al., 2016) and tails (Casarez and Fearing, 2017). Models for robot terrestrial self-righting have considered the transitions between mechanically stable and unstable configurations, potential energy landscapes, and the motions required for the body and legs to coordinate overturning (Peng et al., 2017). In a different context, robot designs inspired by the self-righting abilities of falling cats dynamically reconfigure rotational inertia (inertial morphing) so as to perform rotational reorientations at zero external torque (Cao et al., 2022; Shield et al., 2021). Although this mechanism has also been applied to self-righting robot design (Wang et al., 2022), we are not aware of any studies of animals taking advantage of poses and motions that minimize rotational inertia and hence the torque required to flip upright during terrestrial self-righting (Casarez, 2018).

In this study, we consider terrestrial self-righting by nymphs of the spotted lanternfly (SLF, *Lycorma delicatula*), an invasive insect pest rapidly expanding its range in the U.S. (Urban and Leach, 2022) that falls frequently in response to disturbances and for dispersal (Kim et al.,

2011). (Fig. 1A) In an earlier study, we found that SLF nymphs are highly successful at self-righting dynamically both aerially and during landing (Kane et al., 2021). Here we turn our attention to how SLF nymphs reorient to upright when starting from rest on their backs. SLF nymphs differ from other insect species for which this behavior has been studied (cockroaches (Li et al., 2019), stinkbugs (Pace and Harris, 2021), beetles (Frantsevich, 2004; Zhang et al., 2021), and locusts (Faisal and Matheson, 2001)) in that they have compact, asymmetrical bodies with relatively long legs and, like most robots, they lack wings. We studied SLF nymphs attempting to self-right on several different substrates in order to understand the behaviors used and the underlying mechanisms involved. Based on previous self-righting papers, we hypothesized that the SLFs would choose a mode of righting that coincides with the lowest energy barriers to overturning. In addition, we hypothesized that because they do not have wings, that they would choose strategies to minimize rotational inertia when flipping over.

Building on previous work that made use of 3D rendered models to visualize, animate and perform finite element modeling on extant and extinct organisms (Bishop et al., 2021; Garwood and Dunlop, 2014), we created detailed, posable 3D computer models using photogrammetry and rendering software. Taking inspiration from earlier work on cockroach self-righting using simple geometrical models comprising ellipsoidal bodies, simple wings and one or more rod-like legs, and the energy landscape model (Othayoth and Li, 2021), we then analyzed these models to determine their dynamic inertial properties during self-righting attempts. These models were used in combination with multi-angle high speed video to determine how this species uses its body pose and leg motion to take advantage of energy landscapes and inertial morphing (i.e., how it redistributes its mass to facilitate overturning) during self-righting.

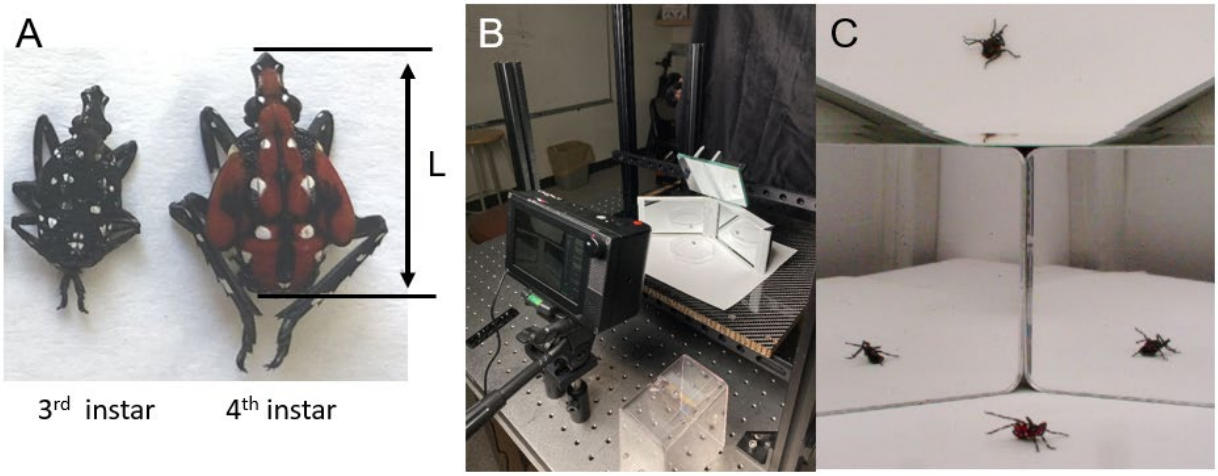

Figure 1. A) Third and fourth instar spotted lanternfly nymphs showing the definition of body length, L. B) Arena and video camera used to film terrestrial self-righting. C) Video frame showing the four camera views recorded of spotted lanternfly nymphs as they attempted to self-right.

Materials and methods

Insect collection, handling & morphometrics

Healthy, intact 3rd and 4th instar SLF nymphs (Fig. 1A) were collected from *Ailanthus altissima* trees and wild grape vines (*Vitis vinifera*) in southeastern Pennsylvania (40°00' 30.2" N, 75°18' 22.0" W) between June 22 and July 9, 2021. All specimens were collected mid-morning through mid-afternoon when they are most active (Kim et al., 2011). Experiments were performed at ambient conditions (23.2 [22.5, 24.1] deg C, and relative humidity 62 [42, 70] %) within 5 minutes of collection to avoid specimen fatigue, hunger, or desiccation. Because SLF are identified as an invasive species and the target of eradication programs (Urban, 2020), all specimens were euthanized by freezing after experimentation.

Morphometric data were measured post-mortem after thawing for ≥ 15 min to preserve tissue hydration and morphology (Aberle et al., 2017). Body mass, M, was measured to ± 0.4 mg using an analytical balance, and body (head-caudal) length, L, was measured to ± 0.05 mm using calipers. (Fig. 1A) We performed experiments on SLF nymphs with life stages determined by coloration, body length and mass (Bien et al., 2023) (3rd instar: 9.2 ± 0.7 mm, 31 ± 11 mg and 4th instar: 11.7 ± 0.8 mm, 59 ± 13 mg; values given as mean ± s.d.). We also dissected 4th instar SLF nymphs (N = 6) to separately measure the mass and dimensions of the legs and body. (Table S1) We did not determine the sex of specimens because an earlier study found only a small (< 4%) difference in median body lengths between sexes for 4th instar nymphs and reported difficulty in determining the sex of 3rd instars (Jang et al., 2013).

Self-righting experiments

Self-righting experiments were performed on a flat, horizontal (± 0.05 deg) white substrate (Fig. 1 B, C) consisting of three materials with different roughness and frictional properties: posterboard (3rd and 4th instars) and spray-painted 80 grit sandpaper and polished glass (4th

instars). (Table 1) SLFs adhere to surfaces using a combination of their tarsal claws and adhesive pads (arolia) (Frantsevich et al., 2008). Tarsal claws have been reported for SLF 3rd and 4th instar nymphs to have > 1 μm radius tips and tip-tip spacing 660-849 μm (Avanesyan et al., 2019). To characterize surface roughness on a length scale relevant for grasping by tarsal claws, we used ImageJ (Schneider et al., 2012) to measure the in-plane diameter of surface features on micrograph images of the sandpaper and posterboard. Polished glass has sub-nm scale roughness (Yates and Duffy, 2008). To characterize the friction between the insect cuticle and substrate that prevents sliding while insects attempt to overturn, freshly euthanized specimens were placed on their dorsal surface on an inclined plane tilted to find the minimum angle, θ, at which sliding first occurs. This was used to compute the coefficient of static friction, $\mu_s = \tan \theta$ for each substrate studied. While we were able to measure multiple trials for glass and posterboard, the frictional force between the insect cuticle and sandpaper was so great that sliding occurred before rolling in only 2 of 83 trials.

Given that arolia of other insects adhere best to smoother substrates (Al Bitar et al., 2010), these results indicate that SLF nymphs placed on glass are likely to adhere using their arolia but not their claws. They also suggest that these insects are likely to be able to hold onto to posterboard using their tarsal claws to penetrate its fibers and to sandpaper by grasping its asperities like a grappling hook. Based on these combined considerations, we expected that SLF nymphs should overturn more effectively on sandpaper than on posterboard and glass.

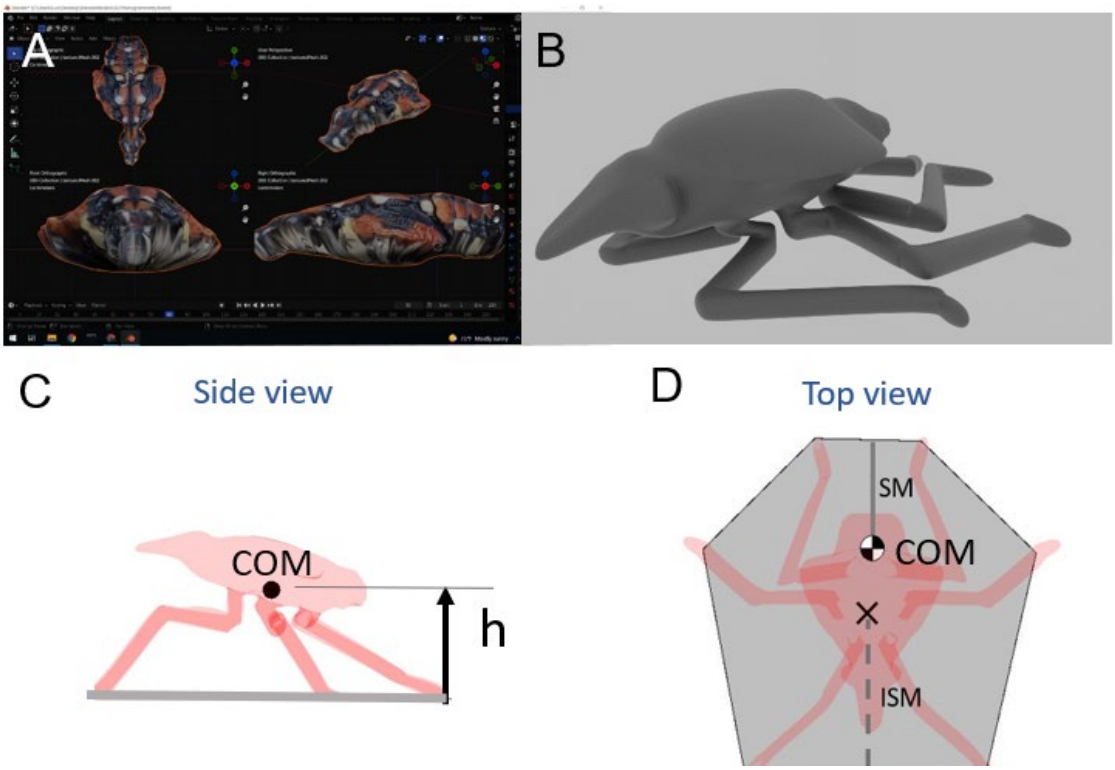

Figure 2. A) Photographs of specimens taken from multiple views were used with photogrammetry software to create detailed 3D models. B) These were used to create posable 3D models in Blender rendering software. C) and D) Spotted lanternfly nymph 3D Blender model (red) and its center of mass (white-and-black circle), shown in side view (C) with COM height, h and top view (D) illustrating the model's support polygon (gray) and its in-plane centroid (X). In D, a gray line indicates the stability margin (SM), and a dashed line the ideal stability margin (ISM).

Substrate	Feature size	Coefficient of static friction (mean ± s.d.)	N specimens (3rd, 4th instars); n trials
Posterboard	40 ± 8 μm diameter fibers (median ± s.d.)	0.36 ± 0.09	10 (5, 5); 63
Glass	< 1 nm[§]	0.55 ± 0.13	9 (5, 4); 73
Sandpaper	570 ± 100 μm diameter pores (mean ± s.d.)	1.2 ± 0.4	2 (1, 1); 2

Table 1: Substrate feature size and coefficients of static friction between the insect cuticle and substrate. [§] Glass roughness reported in (Yates and Duffy, 2008).

Self-righting was measured for 5 trials for each of N = 15 unique individuals for each condition (combination of instar and substrate considered), giving n = 74 trials/condition for all combination of instar and substrate except n = 74 for 4th instars on sandpaper. This design was chosen to minimize the effects of learning, since each specimen experienced at most 5 trials. Following (Faisal and Matheson, 2001), we gently held an SLF nymph briefly to induce tonic immobility, began filming, then placed the SLF nymph on its back on the arena substrate, and allowed it to attempt to self-right for ≤ 30 s. If the specimen failed to self-right in this time window, the trial was terminated and recorded as a failure. An attempt at self-righting was defined as the time from when a specimen on its back began to lift its dorsal side off the ground until it either overturned successfully or else fell on its back after failing to overturn. Successful self-righting was defined as taking place at the moment when a specimen first came to rest stably on all of its feet with its dorsal side up.

High-speed videos were recorded by a Chronos 1.4 video camera (color, 1280 x 1024 pixels, 1000 fps; shutter speed 500 microsec, Krontech, Burnaby, BC, Canada) with a 12 mm focal length lens (f/# = 7, model M1214-MP2, Computar). A total of four views (main camera and three mirror views) were filmed to allow 3D tracking of body parts with minimal occlusion. Data for 3D camera calibrations were obtained using wand calibration with easyWand software (wand score 0.687, reprojection error: 0.46 to 0.74 pixel) (Theriault et al., 201 REF) and the vertical direction determined by dropping a ball on video. The arena was illuminated with an LED light source (SL-200W, Godox, Shenzhen, China) covered by a softbox so as to provide diffuse overhead illumination; the intensity was measured as 7,000 lux at the specimen location, similar to values measured in the understory of trees where SLF nymphs routinely were found.

Repeated viewings of each video and analysis of specific frames were used to determine stereotypical poses assumed while attempting to self-right, the various strategies used for self-righting (i.e., stereotyped sequences of poses used during attempted self-righting) and their frequency and success rate, time spent searching prior to self-righting, number of self-righting attempts, how the legs, feet, and body moved during different behaviors, and how self-righting failed. The mean attempt time was also measured for each specimen as the ratio of the time spent attempting to overturn divided by the number of attempts.

Data analysis and statistical methods

All image processing and data analysis was performed using MATLAB vR2021a with the machine vision, statistics, and curve fitting toolboxes (Mathworks, Natick MA); italicized functions referenced below are from MATLAB. Results are reported as mean [95% CI] unless otherwise noted. Data and code required to reproduce all results are given in Supplemental Dataset S1.

3D modeling and calculations of mechanical properties

To create 3D models, we first performed photogrammetry on SLF 4th instars mounted on foam with a size #00 insect pin and photographed using a Sony DSC-RX100 camera in macro mode under diffuse LED lighting. Images were recorded every 10 deg of horizontal rotation using a turntable to rotate the specimen from 5 different camera elevation angles. The resulting photos were then used in the open-source 3D reconstruction program Meshroom (https://alicevision.org/#meshroom, 1/16/2023) to create a 3D mesh. (Fig. 2A) Following methods outlined in (Semple et al., 2019), the 3D mesh and morphometric data for the body and legs were used with the open-source 3D graphics package Blender (www.blender.org, 1/16/2023) as references for creating a detailed, fully rigged 3D model. (Fig. 2B) The Blender model's accuracy was checked by using it to create and measure the leg and body dimensions of a 3D print to confirm that their relative dimensions agreed with those measured for actual SLF nymphs. The use of a single 3D rendering for modeling the mechanical properties of different size specimens at the two life stages studied here is supported by an earlier growth allometry study which determined that SLF nymphs' body mass scales approximately isometrically with body length (Bien et al., 2023). The body length and mass (L = 8.9 mm, M= 28.4 mg) used for calculations quoted here were typical of 4th instar SLF specimens.

The Blender model was then posed to create an .stl file for each of the body and leg positions observed on video for the various stages during terrestrial self-righting. (See Supplemental Dataset S1 for Blender files and reference photographs.) We treated the head, abdomen and thorax as a single rigid object because we did not observe bending of the body on videos of self-righting (Movie 1). Previous studies have identified the body axes used by other insects during self-righting (Frantsevich, 2004; Li et al., 2019), which we follow here. The orientations of the cranial-caudal (rolling) and lateral (pitching) axes were defined by selecting the head and other body features manually on the Blender model in MATLAB, and a diagonal body axis was

defined as a line passing through one edge of the caudal end at 18 deg to the cranial-caudal axis. (Fig. 3A) The MATLAB package RigidBodyParams (Semechko, 2023) was used to compute the volume and COM coordinates for each Blender model. As a check on the accuracy of the Blender model, we computed a body density 1.0 g/cm^3 from the Blender model's estimated mass and volume, in good agreement with published values for insects (Kühsel et al., 2017). We also checked that the relative masses of the legs and body agreed with our measured values. (Table S1) Custom code was used to compute the convex hull for the .stl file for each pose, yielding the support polygon on which the SLF model rested on the substrate (Ting et al., 1994). This allowed the calculation of the COM height above the flat support plane, h, and the specimen's gravitational potential energy, PE = Mgh, where the acceleration of gravity, g = 9.81 m/s^2. (Fig. 2C) Cross-sections of the anatomical planes were also computed to understand the COM location relative to the body for different stages in self-righting, as well as the geometry of stable vs unstable poses. Body orientation for the 3D model poses was defined by measuring in MATLAB the angle relative to the horizontal of the cranial-caudal axis for pitch, and of the transverse axis for roll. (Fig. 3A) Following Ting and colleagues (Ting, Blickhan and Full, 1994), the stability margin (SM) for each pose was calculated as the shortest distance from the support plane boundaries—defined by the feet in contact with the ground—to the projection of the COM on the support plane, and the percent stability margin from the ratio of the SM to the ideal stability margin (ISM), for which the COM corresponds to the support plane centroid. (Fig. 2C, D)

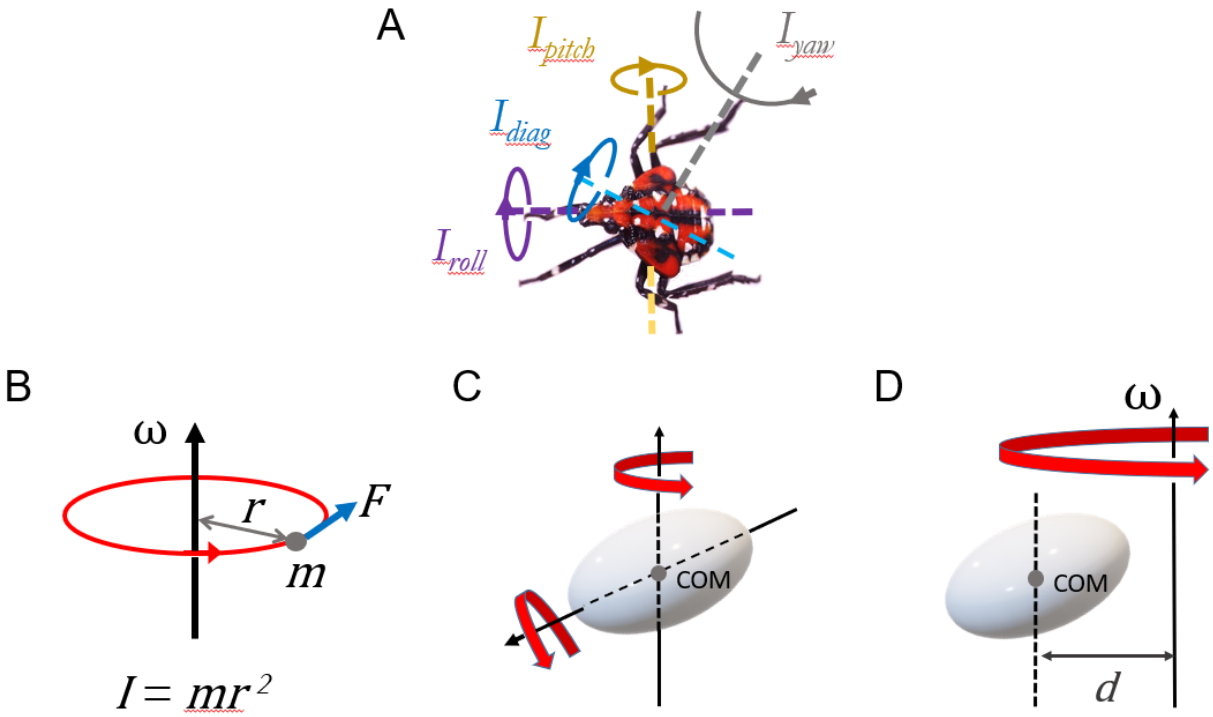

Figure 3. A) Body axes (dashed lines) used during the rotations about the pitch, roll, yaw, and diagonal axes. B) Illustration of the geometry used in defining rotational velocity, ω, force, F, moment arm, r, and the rotational inertia, I, for a point mass, m. C) Rotational inertia depends on the axis of rotation about the center of mass (COM) and D) the distance, d, from the COM to the axis of rotation.

Rotational inertia, *I*, determines an object's resistance to changes in rotational velocity, ω, around a given axis, and the associated torque (moment) via: $\tau = r F = I\, d\omega/dt$, where F = force and r = moment arm. (Fig. 3B) Because rotational inertia depends on both the axis of rotation and its relation to the object's distribution of mass, the rotations of any object about axes passing through its COM are described by three principal axes of stable rotation and three corresponding values of rotational inertia for rotations about each principal axis. (Fig. 3B,C) Given this information, the rotational inertia for any arbitrary axis that passes through the COM can be computed (Marion, 2013). If the axis of rotation corresponding to I_{COM} is shifted so it passes a distance *d* from the COM, then the total rotational inertia, I_{total}, must be computed using the parallel axis theorem (Fig. 3D):

$$I_{total} = I_{COM} + Md^2 \qquad (1)$$

The Blender model for each SLF nymph pose was analyzed using RigidBodyParams to compute the principal axes of rotation and the corresponding moments of inertia, and hence the rotational inertia for the pitch, roll, yaw and diagonal body axes, and the distance *d* from the COM to each rotational axis (Marion, 2013). We also compared the computed body-only pitch rotational inertia, I_{pitch} = 1.29 x 10^{-10} kg m^2, for the Blender model to the measured value, I_{pitch} = 1.86 × 10^{-7} kg m^2, of the cockroach *Blaberus discoidalis* (body mass 225 g and body length 4.4 cm) (Kram et al., 1997). If these insects had the same body geometry, $I_{pitch} \propto ML^2$, then the cockroach to-SLF nymph ratios for I_{pitch} (1.44 × 10^3) and ML^2 (1.94 × 10^3) should agree. In fact, the ratio for pitch rotational inertia is 26% less than predicted by the mass and length ratios, indicating the importance of correcting for the asymmetrical body shape of the SLF nymphs relative to the discoid body of this species of cockroach.

Results

Self-righting strategies

SLF nymphs were found to self-right using a sequence of stereotyped motions similar to three different previously-reported strategies. (Fig. 4A, Movie 1; Table S2, S3) Initially, an overturned SLF nymph lies flat on its back, consistent with the finding that our 3D models have a flat region on their dorsum (Fig. 2B). Upon recovering from tonic immobility, the specimen moves its legs in apparent probing motions laterally and toward its ventral side in apparent attempts to locate a surface (searching). Once a foot makes contact with the substrate dorsally, the other legs are quickly elevated and extended so as to grasp the substrate (planting). Next, the specimen primarily uses its forelegs, with some assistance from the midlegs, to push against the substrate so as to pitch and raise the cranial end off the ground (lifting). The SLF nymph then attempts to flip upright about one of three body axes (overturning), corresponding to the rolling, pitching and diagonal somersaulting strategies previously reported for beetles and cockroaches (Frantsevich, 2004; Li et al., 2019). This was accompanied by a combination of propelling and flailing motions of their legs (Movie 1). Successfully overturned SLF nymphs were observed to readjust their stance to pitch upward to assume the pose typical during resting and walking (righted). Otherwise, they fell upon their backs (failed) and resumed searching.

SLF nymphs self-righted successfully (92-100% all trials) for all three substrates and both life stages studied. (Fig. 4B, Table S2) The most frequently used strategy was diagonal

313 somersaulting (81-99% of trials), in which the SLF nymph rotates about its diagonal axis,
314 pivoting about its caudal end on the edge that was in contact with the substrate. Rolling about
315 an axis on the ground defined either by one side of the body or by two feet planted on one side
316 was less common (1-19% all trials). (Fig. 4C) Only one trial for a single 3rd instar was observed
317 to overturn successfully by pitching about the caudal end while the body was held upright by the
318 hindlegs, accompanied by flailing motions of the forelegs and midlegs toward the ventral side of
319 the body.
320
321 Linear regression was performed to test whether success rate, percent self-righting by diagonal
322 somersaulting, time/attempt and number of attempts considered separately for each condition
323 were correlated with trial number to test the hypothesis that fatigue might cause an increase in
324 the failure rate, time/attempt and number of attempts vs trial number, or conversely, that
325 learning from repeated attempts could make these measures decrease. (Table S4) Only the
326 number of attempts for the 3rd instar nymphs on posterboard increased significantly with trial
327 number. Given this result and the balanced study design, we consequently pooled data across
328 trials and individuals before performing further tests.
329
330 The percent of self-righting trials resulting in success did not depend significantly on instar and
331 substrate (Table S5). All self-righting trials were successful for all 3rd instar specimens for all
332 three substrates and for 4th instar nymphs on sandpaper. All 4th instars succeeded in the first
333 trial and in at least 1 additional trial on posterboard and glass. The only trials in which a
334 specimen failed to eventually self-right involved five failures by two 4th instars on posterboard
335 and five failures by five 4th instars on posterboard on glass. The proportion of successful self-
336 righting by diagonal somersaulting (Table S6) was significantly different for 3rd and 4th instars on
337 posterboard, and for 4th instars on sandpaper vs posterboard and glass, but not for 4th instars on
338 glass and posterboard. Significance testing using Kruskal-Wallis revealed that the total time
339 required to self-right, the time/attempt, and the number of attempts did not depend significantly
340 on condition (substrate and life stage). (Fig. 4D; Table S7)
341

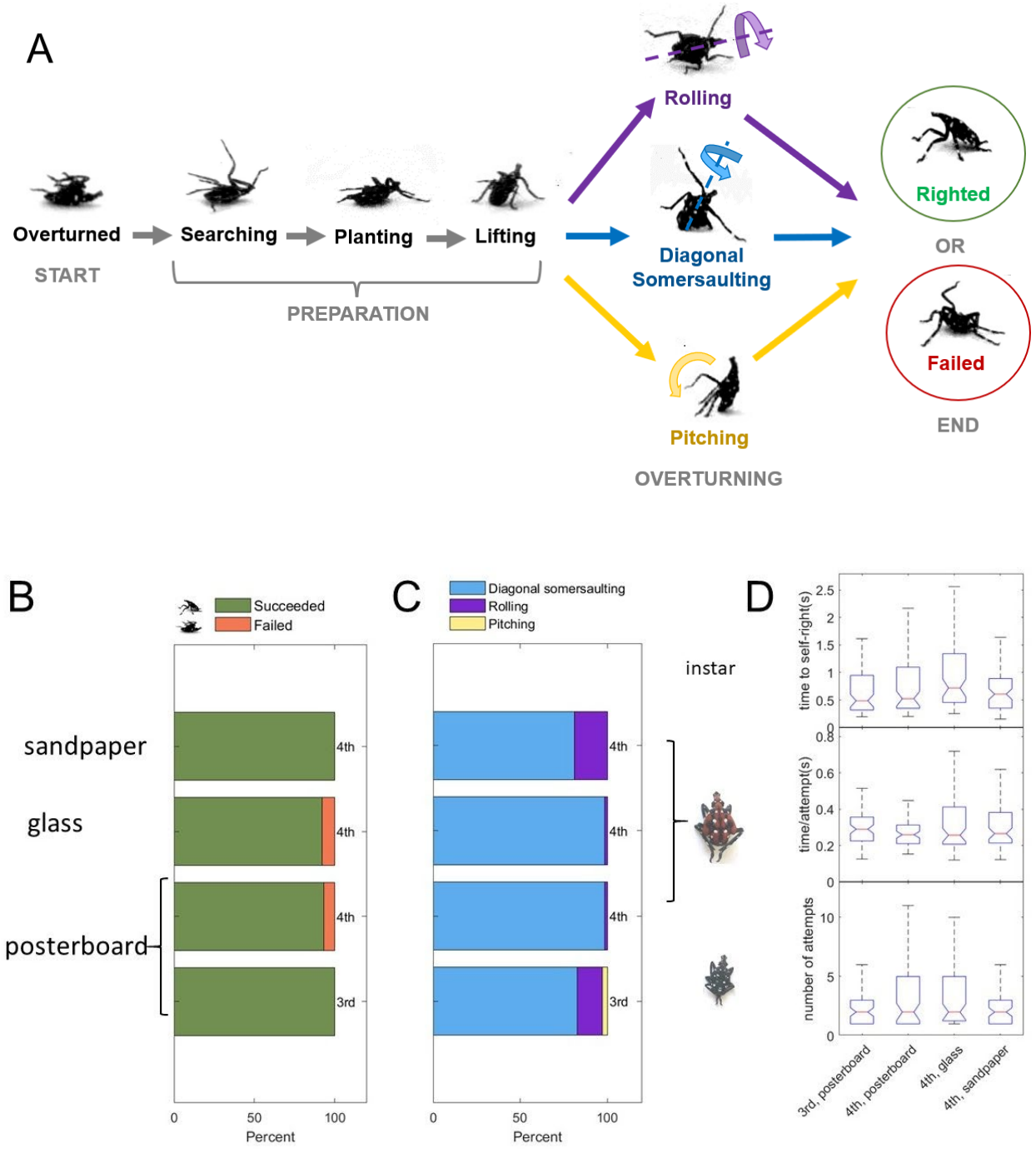

Figure 4. A) Ethogram showing photographs of stereotypical poses assumed during the three methods used for terrestrial self-righting by spotted lanternfly nymphs. Percent successful trials (B) and self-righting strategies (C) used for each combination of substrate and life stage studied. (75 total trials per condition: N = 15, 5 trials/specimen). D) Box-and-whisker plot of time to self-right, time/attempt and number of attempts vs substrate and life stage combinations.

Unsuccessful self-righting occurred when the feet or body slid on the surface, preventing the SLF nymph from getting a secure foothold or from exerting leverage. (Movie 1) For some failed attempts on posterboard, the specimen was successful at lifting its body in an evident attempt to somersault diagonally, but fell back onto its dorsal surface. Another common failure mode during diagonal somersaulting and rolling involved the SLF nymph spinning freely about its yaw axis instead of overturning.

Potential energy and stability

We used the observed stereotypical poses from Fig. 4A to create matching Blender 3D models that were used to compute gravitational potential energy and stability margin for each step during self-righting. (Fig. 5) In addition to the poses shown in Fig. 4A, we created models during overturning of those recorded at 20, 40, 60, and 80% of the time required to self-right. During planting, the SLF nymph abducts and hyperextends its legs (originally held ventral to its body when overturned) dorsally to grip the substrate, thus initially also reducing its PE and increasing the stability margin. The SLF then lifts its body before attempting to overturn, increasing its PE while keeping the stability margin approximately constant. All three self-righting strategies required the specimen to raise its body prior to flipping upright, thereby necessarily increasing PE and reducing its stability margin. Only pitching was found to require overcoming a PE barrier during overturning (Fig. 5A), while only rolling resulted in a negative stability margin (Fig. 5B). Diagonal somersaulting involved neither overcoming a PE barrier nor negotiating a negative stability margin. The final, self-righted SLF nymph is pitched upward upon its legs, resulting in the maximum PE observed for diagonal somersaulting and rolling, while failure (returning to “overturned”) results in a total loss of the PE gained during overturning. Because any PE changes are inelastic, any intermediate reduction in PE results in an energy loss that must be made up before reaching the final upright pose. In other words, the net work required for self-righting is limited by the accumulated positive changes in PE, which is greater for pitching than either rolling or diagonal somersaulting.

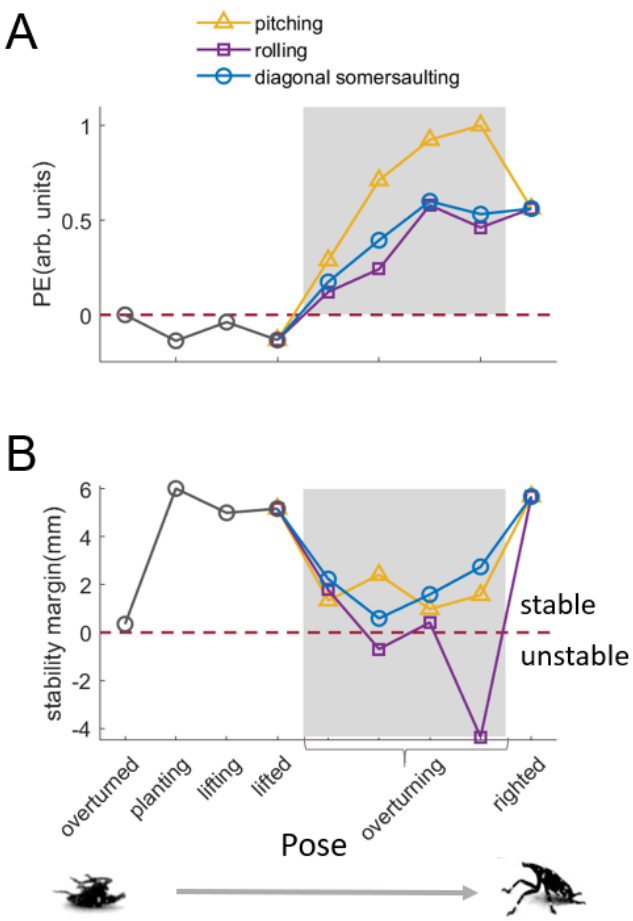

Figure 5. Results of mechanical analysis of the 3D Blender models of a spotted lanternfly nymph in the poses observed during each self-righting strategy used. (A) Gravitational potential energy (PE) and (B) stability margin vs stages during self-righting. The gray shaded region corresponds to the active period of overturning. A negative stability margin indicates that the center of mass falls outside of the base of support, reflecting the instability of the pose.

Rotational properties

To look for evidence that SLF nymphs redistribute their body mass for inertial morphing during self-righting, we also computed the rotational inertia, I_{COM}, for rotations about the body axes and rotational axes of interest of the Blender model based on each of the stereotypical poses. (Table 2; Fig. S1) By comparing values for the body with and without legs, we found that I_{COM} depends substantially on the legs in SLF nymphs, which comprise 30% of total mass. This enables these insects to significantly change their rotational inertia during self-righting by altering their leg positions. In general, the SLF nymphs held their legs such that their principal axes agreed with their body axes to ≤ 12%. During self-righting, I_{yaw} was approximately constant (full range ±15%

mean) and its value was >40% greater than I_{pitch}, I_{roll} and I_{diag}. This enhanced resistance to changes in yawing is relevant because yaw rotations do not contribute to self-righting. Throughout self-righting, values of rotational inertia for the roll and diagonal axis were in close agreement, with their ratio equal to 99.9 ± 5.5% (mean ± s.d.). In spite of this, presumably because these insects tend to hold their bodies with their cranial end pitched upward, even their rolling motions tended to reflect this tendency.

I_{COM} (x 10^{-10} kg m^2)	I_{pitch}	I_{roll}	I_{yaw}	I_{diag}
body with no legs	1.29	0.53	1.58	0.59.
body with legs in righted pose	3.71	3.46	4.90	3.53
Contribution of legs to I_{COM}	188%	559%	211%	493%

Table 2. Rotational inertia about the body center of mass (COM) for the Blender model for rotations about the four axes studied here (Fig 3A), illustrating the effect of including legs in the model.

While there was little difference in I_{COM} for rotations about the roll, pitch, and diagonal axes, the *total* rotational inertia, I_{total}, was different because the rotational axes for pitching & rolling strategies do not pass through the COM (i.e., $d \neq 0$ in Eqn. 1), resulting in increased rotational inertia during overturning using these strategies. (Fig. 6) By contrast, for diagonal somersaulting the rotational axis passes through the COM, so $d \approx 0$, so the total rotational inertial is due only to I_{COM}. Consequently, diagonal somersaulting has the lowest value of I_{total} , and hence the lowest resistance to initiating rotations that can result in overturning.

While we analyzed a single set of characteristic poses for each strategy, the variation in leg and body positions between videos was small compared to the features that determined the main findings here. For example, pitching motions necessarily involve lifting the body COM higher than required for either rolling or diagonal somersaulting, independent of details, so the PE dependence on pose should be invariant to details of the pose. The dimensions relevant for rotational inertia calculations also were similar for the poses used in different videos; for

example, the distance from the pivot point to body COM for rolling and pitching are fixed by body dimensions and the leg positions similar between videos.

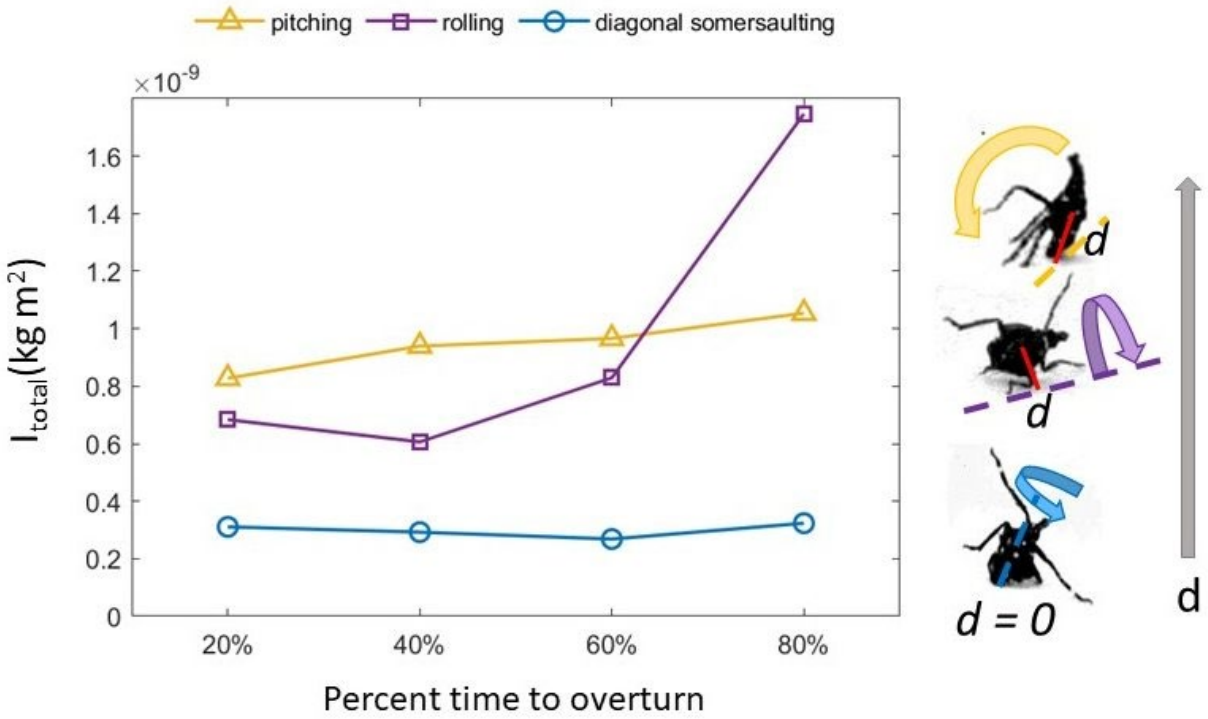

Figure 6. Total rotational inertia, I_{total}, computed from the 3D Blender model for each pose observed during each overturning strategy found for spotted lanternfly. The values shown here for 20, 40, 60 and 80% of the time required to overturn were computed from the same poses considered during overturning in Fig. 5, S1.

Discussion

Spotted lanternfly nymphs were observed to self-right successfully in > 92% trials on all substrates tested using propelling and flailing legs, similar to the high success rates found for most insects in previous studies (Faisal and Matheson, 2001; Frantsevich, 2004; Li et al., 2019; Pace and Harris, 2021; Zhang et al., 2021). We found several other similarities between the terrestrial self-righting behaviors of SLF nymphs and other insect species. Before overturning, SLF nymphs initially used searching and planting motions similar to those described for beetles as well as for spiders (Frantsevich, 2004; O'Donnell, 2018). SLF nymphs employed three self-righting strategies similar to those used by some cockroaches and beetles (Frantsevich, 2004; Li et al., 2019). The time required for self-righting was similar to that reported for locusts (Faisal

and Matheson, 2001), stink bugs *Halyomorpha halys* (Pace and Harris, 2021) and beetles (Zhang et al., 2021).

There were also some striking differences between species. While the strategies used by beetles and stink bugs (Pace and Harris, 2021; Sasaki and Nonaka, 2016; Zhang et al., 2021) and the times required for overturning by beetles (Zhang et al., 2021) depended significantly on substrate properties, SLF nymphs favored diagonal somersaulting for all three substrates studied and their self-righting times did not depend on substrate. These results likely reflect this species' ability to cling tenaciously to a wide variety of substrates using a combination of their tarsal claws and arolia (Avanesyan et al., 2019; Kane et al., 2021; Kim et al., 2011). It also may reflect the fact that almost all other insect species previously studied were able to employ wings as an aid on smoother surfaces. Diagonal somersaulting may make an asset out of low friction by enabling the insect to pivot about its caudal end.

We also considered whether these results can be explained using 3D Blender models to compute the suite of mechanical properties considered here. Overturning by any method was found to require an increase of gravitational PE to lift the body COM to its walking pose. However, the predominant strategy (diagonal somersaulting) lacked a gravitational PE barrier to overturning as well as having the lowest total rotational inertia and a stability margin greater than or equal to that for the other two strategies. While rolling required a similar PE increase to diagonal somersaulting and also lacked a PE barrier, it also had a greater total rotational inertia than diagonal somersaulting and lower stability margin than the other two strategies. Pitching, which was only observed in one trial, corresponded to both a PE barrier and high total rotational inertia. Because yawing was found to be a common failure mode, we were interested to find that specimens were able to configure their bodies such that their yaw moment of inertia exceeded that for other rotations that could contribute to overturning.

This study's results show that combining multiple measures of 3D Blender models (energy landscape, stability margins, and rotational properties) during each stage of terrestrial self-righting gives a fuller explanation of why SLF nymphs use the observed distribution of strategies than any single quantity alone. They also point to the likely importance of considering rotational inertia when analyzing complex animal behaviors in general. The importance of using detailed, realistic models confirmed the finding that the legs constitute such large fraction of the total mass that their configuration is important for understanding how their relevant mechanical

properties depend on limb pose. The observed asymmetrical body motions also indicate the importance of characterizing the asymmetrical body morphology and leg usage in detail. On a practical note, we also provide an accessible, low-cost template for creating 3D models of insect external morphology using free software packages and low-cost photogrammetry for studies that do not require the resolution and full 3D imaging capabilities of microCT and specimens too small for 3D scanning.

In future work, it would be interesting to see if these results for self-righting generalize to a wider range of insect species and morphologies. For example, (Li et al., 2019) has suggested that potential energy barriers are necessarily higher for pitching than rolling and those for diagonal axes intermediate for elongated bodies where elongation = body length/width, and that this likely influences the choice of strategy used. However, this model does not take into account the effect of appendages (e.g., legs, wings and antenna) and the likelihood that the total rotational inertia should increase faster for pitching than rolling as elongation increases. Future research could explore whether the addition of these other perspectives can explain the complex range of self-righting behaviors reported for insects with bodies that range from compact (e.g., ladybird beetles (Zhang et al., 2021)) to extremely slender (e.g., stick insects (Graham, 1979)). While we have used a sequence of 3D models for stereotypical poses sampled regularly during the behavior of interest, future work could also explore animating the rendered models using actual body coordinates determined by tracking 3D video. This would allow the extension of these methods to exploring a wider range of motions (e.g., modes of locomotion) than those considered here, as well as the creation of 3D prints (Behm et al., 2018) that can be used for in vitro experimentation and robotics.

Acknowledgements

We thank Robert Beyer and Kent Watson for instrumental design and fabrication assistance.

Competing interests

No competing interests declared.

Funding

Haverford College, National Science Foundation CAREER award to STH (IOS-1453106).

Data availability

All data and code required to reproduce all results and figures is included in Supplemental Dataset S1.

References

Aberle, B., Jemmali, R. and Dirks, J.-H. (2017). Effect of sample treatment on biomechanical properties of insect cuticle. *Arthropod Structure & Development* **46**, 138–146.

Al Bitar, L., Voigt, D., Zebitz, C. P. W. and Gorb, S. N. (2010). Attachment ability of the codling moth Cydia pomonella L. to rough substrates. *Journal of Insect Physiology* **56**, 1966–1972.

Avanesyan, A., Maugel, T. K. and Lamp, W. O. (2019). External morphology and developmental changes of tarsal tips and mouthparts of the invasive spotted lanternfly, Lycorma delicatula (Hemiptera: Fulgoridae). *PLoS One* **14**,.

Behm, J. E., Waite, B. R., Hsieh, S. T. and Helmus, M. R. (2018). Benefits and limitations of three-dimensional printing technology for ecological research. *BMC Ecol* **18**, 32.

Bien, T., Alexander, B. H., White, E., Hsieh, S. T. and Kane, S. A. (2023). Sizing up spotted lanternfly nymphs for instar determination and growth allometry. *PLOS ONE* **18**, e0265707.

Bishop, P. J., Cuff, A. R. and Hutchinson, J. R. (2021). How to build a dinosaur: Musculoskeletal modeling and simulation of locomotor biomechanics in extinct animals. *Paleobiology* **47**, 1–38.

Bolmin, O., Duan, C., Urrutia, L., Abdulla, A. M., Hazel, A. M., Alleyne, M., Dunn, A. C. and Wissa, A. (2017). Pop! Observing and Modeling the Legless Self-righting Jumping Mechanism of Click Beetles. In *Biomimetic and Biohybrid Systems* (ed. Mangan, M.), Cutkosky, M.), Mura, A.), Verschure, P. F. M. J.), Prescott, T.), and Lepora, N.), pp. 35–47. Cham: Springer International Publishing.

Brackenbury, J. (1990). A novel method of self-righting in the springtail Sminthurus viridis (Insecta: Collembola). *Journal of Zoology* **222**, 117–119.

Cao, J., Wang, S., Zhu, X. and Song, L. (2022). A Review of Research on Falling Cat Phenomenon and Development of Bio-Falling Cat Robot. In *2022 WRC Symposium on Advanced Robotics and Automation (WRC SARA)*, pp. 160–165.

Casarez, C. S. (2018). *Tail-Augmented Self-Righting and Turning of a Dynamic Legged Millirobot*. University of California, Berkeley.

Casarez, C. S. and Fearing, R. S. (2017). Dynamic terrestrial self-righting with a minimal tail. In *2017 IEEE/RSJ International Conference on Intelligent Robots and Systems (IROS)*, pp. 314–321.

Domokos, G. and Várkonyi, P. L. (2007). Geometry and self-righting of turtles. *Proceedings of the Royal Society B: Biological Sciences* **275**, 11–17.

Faisal, A. A. and Matheson, T. (2001). Coordinated righting behaviour in locusts. *Journal of Experimental Biology* **204**, 637–648.

Frantsevich, L. (2004). Righting kinematics in beetles (Insecta: Coleoptera). *Arthropod structure & development* **33**, 221–235.

Frantsevich, L., Ji, A., Dai, Z., Wang, J., Frantsevich, L. and Gorb, S. N. (2008). Adhesive properties of the arolium of a lantern-fly, Lycorma delicatula (Auchenorrhyncha, Fulgoridae). *Journal of Insect Physiology* **54**, 818–827.

Full, R., Yamauchi, A. and Jindrich, D. (1995). Maximum single leg force production: cockroaches righting on photoelastic gelatin. *Journal of Experimental Biology* **198**, 2441–2452.

Garwood, R. and Dunlop, J. (2014). The walking dead: Blender as a tool for paleontologists with a case study on extinct arachnids. *Journal of Paleontology* **88**, 735–746.

Graham, D. (1979). Effects of circum-oesophageal lesion on the behaviour of the stick insect Carausius morosus. *Biol. Cybernetics* **32**, 139–145.

Jang, Y., An, H.-G., Kim, H. and Kim, K.-H. (2013). Spectral preferences of Lycorma delicatula (Hemiptera: Fulgoridae). *Entomological Research* **43**, 115–122.

Kane, S. A., Bien, T., Contreras-Orendain, L., Ochs, M. F. and Tonia Hsieh, S. (2021). Many ways to land upright: novel righting strategies allow spotted lanternfly nymphs to land on diverse substrates. *Journal of The Royal Society Interface* **18**, 20210367.

Kim, J. G., Lee, E.-H., Seo, Y.-M. and Kim, N.-Y. (2011). Cyclic Behavior of Lycorma delicatula (Insecta: Hemiptera: Fulgoridae) on Host Plants. *J Insect Behav* **24**, 423.

Kram, R., Wong, B. and Full, R. J. (1997). Three-dimensional kinematics and limb kinetic energy of running cockroaches. *The Journal of Experimental Biology* **200**, 1919–1929.

Kühsel, S., Brückner, A., Schmelzle, S., Heethoff, M. and Blüthgen, N. (2017). Surface area–volume ratios in insects. *Insect Science* **24**, 829–841.

Li, C., Kessens, C. C., Young, A., Fearing, R. S. and Full, R. J. (2016). Cockroach-inspired winged robot reveals principles of ground-based dynamic self-righting. In *2016 IEEE/RSJ International Conference on Intelligent Robots and Systems (IROS)*, pp. 2128–2134.

Li, C., Wöhrl, T., Lam, H. K. and Full, R. J. (2019). Cockroaches use diverse strategies to self-right on the ground. *Journal of Experimental Biology* **222**, jeb186080.

Malashichev, Y. B. (2006). One-sided limb preference is linked to alternating-limb locomotion in anuran amphibians. *Journal of Comparative Psychology* **120**, 401–410.

Marion, J. B. (2013). *Classical dynamics of particles and systems*. Academic Press.

O'Donnell, D. (2018). *Mechanics of righting behavior in the tarantula (Theraphosidae)*. Wake Forest University.

Othayoth, R. and Li, C. (2021). Propelling and perturbing appendages together facilitate strenuous ground self-righting. *eLife* **10**, e60233.

Pace, C. M. and Harris, M. (2021). Flat on its back: the impact of substrate on righting methods of the brown marmorated stink bug, Halyomorpha halys. *J Comp Physiol A*.

Pellis, V. C., Pellis, S. M. and Teitelbaum, P. (1991). A descriptive analysis of the postnatal development of contact-righting in rats (Rattus norvegicus). *Developmental Psychobiology* **24**, 237–263.

Peng, S., Ding, X., Yang, F. and Xu, K. (2017). Motion planning and implementation for the self-recovery of an overturned multi-legged robot. *Robotica* **35**, 1107–1120.

Robins, A., Lippolis, G., Bisazza, A., Vallortigara, G. and Rogers, L. J. (1998). Lateralized agonistic responses and hindlimb use in toads. *Animal Behaviour* **56**, 875–881.

Saranli, U., Rizzi, A. A. and Koditschek, D. E. (2004). Model-Based Dynamic Self-Righting Maneuvers for a Hexapedal Robot. *The International Journal of Robotics Research* **23**, 903–918.

Sasaki, M. and Nonaka, T. (2016). The Reciprocity of Environment and Action in Self-Righting Beetles: The Textures of the Ground and an Object, and the Claws. *Ecological Psychology* **28**, 78–107.

Schneider, C. A., Rasband, W. S. and Eliceiri, K. W. (2012). NIH Image to ImageJ: 25 years of image analysis. *Nature Methods* **9**, 671–675.

Semechko, A. (2023). Rigid body parameters of closed surface meshes. *GitHub*.

Semple, T. L., Peakall, R. and Tatarnic, N. J. (2019). A comprehensive and user-friendly framework for 3D-data visualisation in invertebrates and other organisms. *Journal of Morphology* **280**, 223–231.

Shield, S., Jericevich, R., Patel, A. and Jusufi, A. (2021). Tails, Flails, and Sails: How Appendages Improve Terrestrial Maneuverability by Improving Stability. *Integrative and Comparative Biology* **61**, 506–520.

Silvey, G. E. (1973). Motor Control of Tail Spine Rotation of the Horseshoe Crab, Limulus Polyphemus. *Journal of Experimental Biology* **58**, 599–625.

Ting, L. H., Blickhan, R. and Full, R. J. (1994). Dynamic and static stability in hexapedal runners. *Journal of Experimental Biology* **197**, 251–269.

Urban, J. M. (2020). Perspective: shedding light on spotted lanternfly impacts in the USA. *Pest Management Science* **76**, 10–17.

Urban, J. M. and Leach, H. (2022). Biology and Management of the Spotted Lanternfly, Lycorma delicatula (Hemiptera: Fulgoridae), in the United States. *Annual Review of Entomology* **68**,.

Wang, S., Wang, K., Zhang, C. and Dai, J. S. (2022). Kinetostatic backflip strategy for self-recovery of quadruped robots with the selected rotation axis. *Robotica* **40**, 1713–1731.

Xuan, Q. and Li, C. (2020a). Coordinated appendages accumulate more energy to self-right on the ground. *IEEE Robotics and Automation Letters* **5**, 6137–6144.

Xuan, Q. and Li, C. (2020b). Randomness in appendage coordination facilitates strenuous ground self-righting. *Bioinspiration & Biomimetics* **15**, 065004.

Yates, B. W. and Duffy, A. M. (2008). Statistical analysis of the metrological properties of float glass. In *Advances in X-Ray/EUV Optics and Components III*, pp. 105–115. SPIE.

Zhang, J., Li, J., Li, C., Wu, Z., Liang, H. and Wu, J. (2021). Self-righting physiology of the ladybird beetle Coccinella septempunctata on surfaces with variable roughness. *Journal of Insect Physiology* **130**, 104202.

Figure captions

Figure 1. A) First and second instar spotted lanternfly nymphs showing the definition of body length, L. B) Arena and video camera used to film terrestrial self-righting. C) Video frame showing the four camera views recorded of spotted lanternfly nymphs as they attempted to self-right.

Figure 2. A) Photographs of specimens taken from multiple views were used with photogrammetry software to create detailed 3D models. B) These were used to create posable 3D models in Blender rendering software. C) and D) Spotted lanternfly nymph 3D Blender

model (red) and its center of mass (white-and-black circle), shown in side view (C) with COM height, h and top view (D) illustrating the model's support polygon (gray) and its in-plane centroid (X). In D, a gray line indicates the stability margin (SM), and a dashed line the ideal stability margin (ISM).

Figure 3. A) Body axes (dashed lines) used during the rotations about the pitch, roll, yaw, and diagonal axes. B) Illustration of the geometry used in defining rotational velocity, ω, force, F, moment arm, r, and the rotational inertia, I, for a point mass, m. C) Rotational inertia depends on the axis of rotation about the center of mass (COM) and D) the distance, d, from the COM to the axis of rotation.

Figure 4. A) Ethogram showing photographs of stereotypical poses assumed during the three methods used for terrestrial self-righting by spotted lanternfly nymphs. Percent successful trials (B) and self-righting strategies (C) used for each combination of substrate and life stage studied. (75 total trials per condition: N = 15, 5 trials/specimen). D) Box-and-whisker plot of time to self-right, time/attempt and number of attempts vs substrate and life stage combinations.

Figure 5. Results of mechanical analysis of the 3D Blender model of a spotted lanternfly nymph in the poses observed during each self-righting strategy used. Gravitational potential energy (PE) (A) and stability margin (B) are shown vs body pose. Negative values for the stability indicate poses unstable to overturning. The gray shaded region corresponds to the active period of overturning.

Figure 6. Results of mechanical analysis of the 3D Blender model of a spotted lanternfly nymph in the poses observed during each self-righting strategy used. Gravitational potential energy (PE) (A) and stability margin (B) are shown vs body pose. (The values shown here for 20, 40, 60 and 80% of the time required to overturn were computed from the same poses considered during overturning in Fig. 3A, S1.)